Research article

Mengyuan Ma[a], Jiantian Zhang[a], Yao Zhang, Xiaoli Wang, Junli Wang*, Peng Yu, Zheng Liu and Zhiyi Wei

Ternary chalcogenide Ta_2NiS_5 nanosheets for broadband pulse generation in ultrafast fiber lasers

https://doi.org/10.1515/nanoph-2019-0350
Received September 7, 2019; revised November 4, 2019; accepted November 5, 2019

Abstract: In this article, a high-quality saturable absorber (SA) based on a two-dimensional ternary chalcogenide Ta_2NiS_5 nanosheet has been successfully fabricated and used in 1- and 1.5-μm spectral regions to generate ultrafast laser pulses. The Ta_2NiS_5-based SA is fabricated by mechanical exfoliation and sandwiched between two fiber ferrules to form a fiber-compatible SA. On the basis of the twin-detector technique, nonlinear optical absorption of the Ta_2NiS_5-SA is characterized by 64.7% and 11.95% modulation depths with 1.3 and 0.72 MW/cm^2 saturation intensities at 1028 and 1570 nm, respectively. When Ta_2NiS_5-SA is integrated into Yb- and Er-doped fiber laser cavities, stable self-starting Q-switched pulses are observed. Furthermore, by adjusting the cavity structure and optimizing dispersion in the cavity, we obtain hybrid mode-locking and mode-locking fiber laser operation at 1029 and 1569 nm, respectively. These results validate the performance of Ta_2NiS_5 as a broadband SA for the generation of ultrafast laser pulses, offering new opportunities of ternary transition-metal dichalcogenide alloys in future photonic devices.

Keywords: fiber laser; Q-switched; mode-locked.

[a]**Mengyuan Ma and Jiantian Zhang:** These authors contributed equally.
***Corresponding author: Junli Wang,** School of Physics and Optoelectronics Engineering, Xidian University, Xian, China, e-mail: dispersion@126.com. https://orcid.org/0000-0003-1718-5024
Mengyuan Ma, Yao Zhang and Xiaoli Wang: School of Physics and Optoelectronics Engineering, Xidian University, Xian, China
Jiantian Zhang and Peng Yu: School of Materials Science and Engineering, Sun Yat-sen University, Guangzhou, China
Zheng Liu: Center for Programmable Materials, School of Materials Science and Engineering, Nanyang Technological University, 50 Nanyang Avenue, 639798 Singapore, Singapore
Zhiyi Wei: Beijing Nation Laboratory for Condensed Matter Physics, Institute of Physics, Chinese Academy of Sciences, 100190 Beijing, China

1 Introduction

The increasing requirements of pulsed fiber lasers in scientific research and industrial applications have stimulated the continuous exploration of novel saturable absorbers (SAs) [1–4], which are compact and low-cost nonlinear optical elements that convert the continuous wave into a train of ultrashort optical pulses [5–7]. The use of SAs has become an effective approach to accumulate enough nonlinear phase shift without lengthening the cavity of fiber lasers [8–10]. Traditional SAs, such as semiconductor saturable absorber mirrors, have narrow wavelength tuning ranges and are complex components for fabrication [11]. Since the first use of atomic-layer graphene to mode-lock fiber lasers [12], researchers have been paying much attention to the investigation and application of new 2D materials in ultrafast photonics. Another 2D material, black phosphorus (BP), has its own layer-dependent direct bandgap (0.3–1.5 eV) [13, 14], which can be used in the infrared band [15–17]. However, the stability of BP is a major obstacle in its applications [18]. Up to now, with the advancement of materials science, new nanomaterials such as antimonene [4] and transition-metal dichalcogenides (TMDs) (MoS_2 [19], WSe_2 [20], SnS_2 [21]) have experienced rapid development because of their large third-order optical nonlinearity and ultrafast carrier dynamics [22, 23].

To date, 2D ternary materials have been extensively studied because of their unique structures with the addition of a third element. Ternary materials provide more freedom to tune their physical properties by changing the proportion of the elements [24]. As a member of the ternary chalcogenide family, the quasi-one-dimensional (1D) material Ta_2NiS_5 exhibits not only 2D properties with a layered crystalline structure stacked by weak van der Waals interactions but also 1D properties with chain structures in individual layers [25, 26]. The structure of Ta_2NiS_5 can be characterized by a series of zigzag wave chains, in

which $[TaS_6]_2$ dimer chains consisting of two $[TaS_6]$ octahedral single chains are periodically interconnected with NiS_4 tetrahedral single chains [24]. This chain structure leads to strong in-plane anisotropy in Ta_2NiS_5. Bulk and monolayer Ta_2NiS_5 are both semiconductors with a direct bandgap of 0.36 and 0.39 eV, respectively, indicating that few-layer Ta_2NiS_5 is likely to be used in broadband functional photoelectric devices [27].

Monolayer or few-layer SAs can be produced through a variety of methods, such as mechanical exfoliation [28], liquid-phase exfoliation (LPE) [29], and chemical vapor deposition (CVD) [30–32]. The nonlinear saturable absorption properties of few-layer Ta_2NiS_5 have been studied by Yan et al. for LPE [33]. However, they only achieved Q-switched pulse at 1.9 μm in an all-solid-state laser.

In this article, we propose and experimentally demonstrate that fiber lasers (i.e. Yb- and Er-doped) can be Q-switched and mode-locked by exploiting the broadband saturable absorption of the ternary chalcogenide Ta_2NiS_5. The modulation depth of Ta_2NiS_5-SA is 64.7% at 1028 nm and 11.9% at 1570 nm. To the best of our knowledge, this is the first report where Ta_2NiS_5 as an SA is used to achieve ultrafast pulse generation in all-fiber Yb- and Er-doped lasers, which underscores its applicability as a broadband SA material.

2 Fabrication and characterization of Ta_2NiS_5-SA

Bulk crystals of Ta_2NiS_5 were synthesized by the chemical vapor transport (CVT) method. Ta/Ni/S in the molar ratio 2:1:5 giving a total weight of 0.3 g was mixed with 10 mg of iodide and sealed in an evacuated quartz tube. The sealed tube was placed in a three-zone furnace. The growth zone was pre-reacted at 800°C for 30 h and kept for 6 days. The reaction zone was pre-reacted at 500°C for 30 h and then at 880°C for 3 days. Finally, the furnace was naturally cooled down to room temperature and then the single crystals were collected.

Ta_2NiS_5 crystal belongs to the orthorhombic space group *Cmcm* (63) and is a layered compound [26]. The structure of Ta_2NiS_5, based on *Inorganic Crystal Structure Database*, is shown in Figure 1A and B, indicating that the layers are composed of distorted NiS_4 tetrahedra and TaS_6 octahedra connected to each other by sharing S-S edges, which are bonded by weak van der Walls forces. In addition, the thickness of a single layer of Ta_2NiS_5 calculated from the structure is 0.63 nm [26]. Single crystals of Ta_2NiS_5, which are typically a few millimeters long and about 0.1 mm wide (inset in Figure 1C), were grown by CVT from their elementary powders [34]. The X-ray diffraction (XRD) patterns of the powder confirmed that the as-synthesized crystals were Ta_2NiS_5 crystals (Figure 1C).

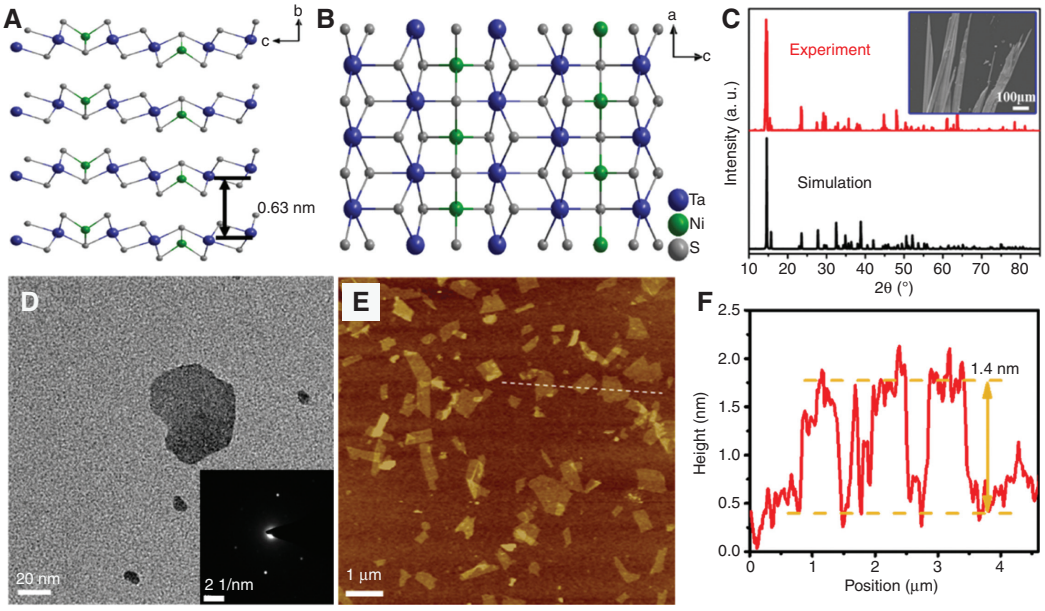

Figure 1: Characterization of Ta_2NiS_5.
Structures of Ta_2NiS_5 viewed (A) from the *a*-axis and (B) from the *b*-axis. (C) XRD pattern of Ta_2NiS_5 layered microflake. Inset: SEM image. (D) TEM image of a typical Ta_2NiS_5 nanosheet. Inset: The corresponding SAED pattern. (E) AFM image and (F) height profile along the white imaginary line in (E).

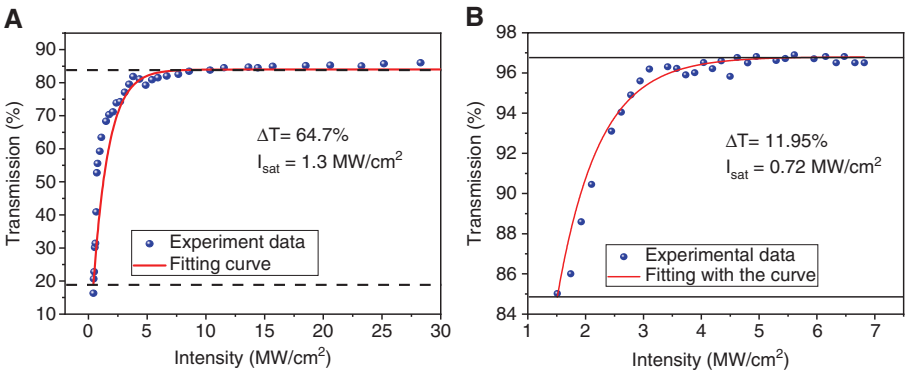

Figure 2: Ultrafast-optical property of Ta_2NiS_5-SA.
Nonlinear optical transmission of SA at (A) 1 μm and (B) 1.5 μm.

More details on the synthesis procedure are given in Experimental Section of Ref. [34].

Ta_2NiS_5 nanosheets were prepared by micromechanical exfoliation. Transmission electron microscopy (TEM) image (Figure 1D) and atomic force microscopy (AFM) height topography (Figure 1E) demonstrate the layered structure of the Ta_2NiS_5 nanosheets. Inset in Figure 1D shows the corresponding selected-area electron diffraction (SAED) of the Ta_2NiS_5 nanosheet, giving clear bright spots, which confirms its single-crystalline structure. AFM measurements revealed that the thickness of exfoliated Ta_2NiS_5 nanosheets was ~1.4 nm.

The nonlinear optical absorption of the Ta_2NiS_5 was characterized using the twin-detector technique reported in our previous work [35]. A home-made passively mode-locked fiber laser operating at 1028 nm was used as the pump light (6.6 ps pulse duration, 35.95 MHz pulse repetition rate). From measurements and curve-fitting, the following SA parameters were extracted: saturation intensity I_{sat} ~ 1.3 MW/cm² and modulation depth αs ~ 64.7% at 1028 nm (Figure 2A). The same measurements were also carried out at 1570 nm (246 fs pulse duration, 50.18 MHz pulse repetition rate). The measured parameters were I_{sat} ~ 0.72 MW/cm² and αs ~ 11.95% (Figure 2B). Thus, Ta_2NiS_5-SA shows saturable absorption in both wavelengths.

3 Ytterbium-doped 1-μm fiber laser

The demonstrated saturable absorption of the Ta_2NiS_5 at 1030 nm indicates that the device could be used to generate a regular train of Q-switched and mode-locked pulses in this spectral region. The experimental setup is shown in Figure 3. A LD laser (VLSS, Connet, Shanghai, China) emitting at 976 nm with a maximum output power

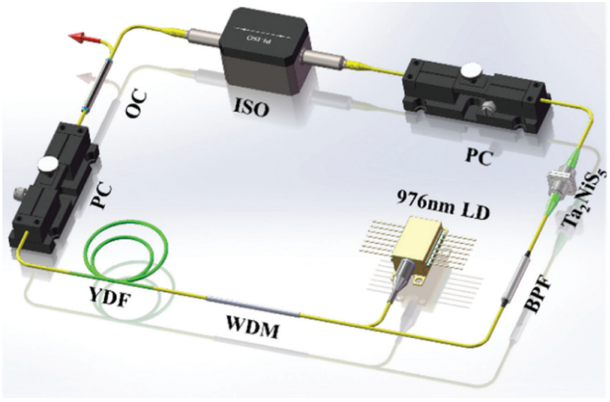

Figure 3: Schematic of ytterbium-doped fiber laser setup.

of 600 mW was used as the pump source. The pump light was launched into the laser cavity using a 980/1030 nm wavelength-division multiplexing (WDM; 980/1030-HF-B-05-NE, OF-Link, Suqian, China) coupler. A 28-cm-long Yb-doped single-mode fiber (Liekki Yb 1200-4/125, Vancouver, WA, USA) was used as the gain medium. Two polarization controllers (PCs) (FPC-200, OZ Optics, Jiaxing, China) were used to optimize the Q-switching and mode-locking operation as well as the intracavity birefringence. The Ta_2NiS_5-SA device was placed after the PCs. A polarization-independent isolator (PIISO-1030, OF-Link, Suqian, China) was used to ensure unidirectional propagation. An 8-nm bandpass filter (BPF; BPF-1030, OF-Link, Suqian, China) was added to the cavity for wavelength selection. A coupler (SR4889, AFR, Zhuhai, China) with 10% output was employed to output the laser.

The output was connected to an optical spectrum analyzer (Ocean Optics HR2000, Shanghai, China), a commercial autocorrelator (APE Pulse Check USB, Berlin, Germany), an RF spectrum analyzer (Tektronix RSA5103B, Shanghai, China), and a real-time oscilloscope (Tektronix

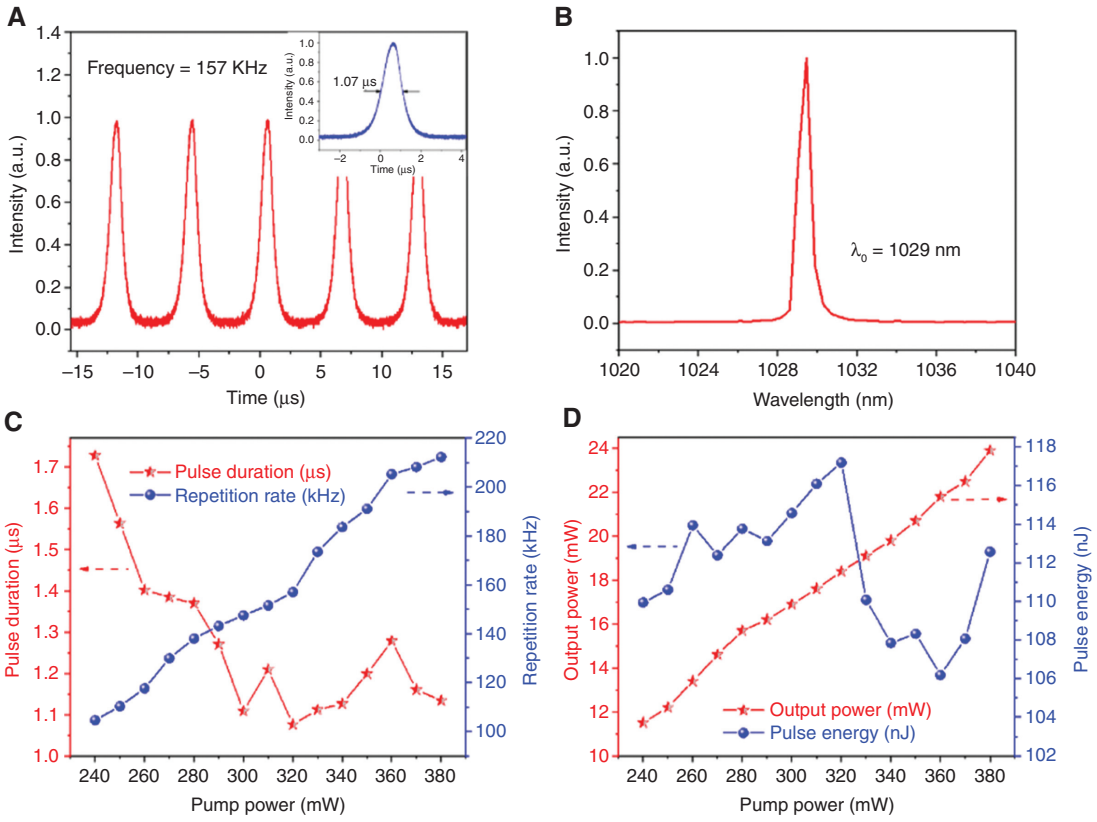

Figure 4: The results of Q-switched YDFL.
(A) Q-switched pulse width at the pump power of 320 mW. (B) Optical spectrum. (C) Pulse repetition rate and pulse duration vs. pump power. (D) Single-pulse energy and average output power vs. pump power.

DPO3053, 500 MHz, 2.5 GS/S, Shanghai, China) together with a photodetector (Thorlabs DET10A/M, Shanghai, China) to allow measurements of the spectra and the pulse train.

3.1 Q-switched ytterbium-doped fiber laser (YDFL) with Ta_2NiS_5 SA

Figures 4A shows a typical Q-switched pulse train of the Ta_2NiS_5 SA. The pulse trains are shown for a pump power of 320 mW in the insert of Figure 4A, where the minimum pulse width is 1.07 μs. The optical spectrum at a pump power of 320 mW is shown in Figure 4B. The central wavelength of the laser signal is located at 1029 nm. The modulation range of the repetition rate and the full width at half-maximum (FWHM) of the pulse duration were found to be 104.6–212.3 kHz and 1.72–1.13 μs, respectively, by changing the pump power, as shown in Figure 4C. Figure 4D plots the pulse output power and the pulse energy of Q-switching vs. the pump power. With the increase of the pump power from 240 to 380 mW, the pulse output power and the pulse energy changed to 11.5–23.9 mW and 109.9–112.5 nJ, respectively, with the maximum pulse energy of 117.2 nJ.

3.2 Hybrid mode-locking YDFL with Ta_2NiS_5 SA

Although we obtained a stable Q-switched pulse train, no mode-locking phenomenon was observed when we increased the pump power and adjusted the PCs. During subsequent experiments, we found that the output power in the cavity was low and the fluorescence brightness of the gain fiber was abnormal. Therefore, we removed all the connected fiber ferrules in the cavity, replaced them with direct fiber fusion, and checked all the melting points. In the experiment using the polarization-independent isolator to study the separate mode-locking of materials, we only observed the mode-locking signs but could not obtain stable mode-locked output. Therefore, the polarization-dependent isolator was replaced and the mode-locking was assisted by NPE.

With the suitable state of PC and a pump power of 180 mW, stable passive mode-locking operation was obtained. Figure 5A shows the typical spectrum of the

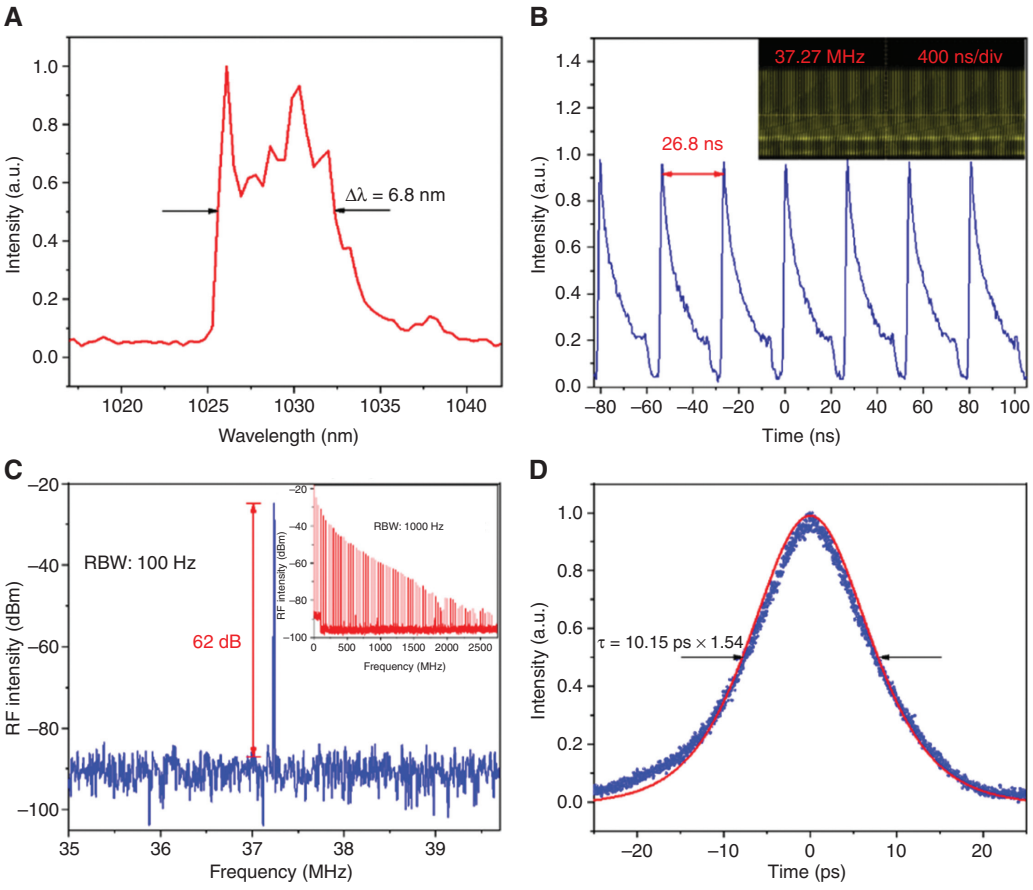

Figure 5: The results of hybrid mode-locking YDFL.
(A) Optical spectrum. (B) Pulse trains of mode-locking operation at pump power of 320 mW. Inset: Oscilloscope traces.
(C) RF spectra. (D) Autocorrelation trace for the output pulse.

mode-locked fiber laser. Here, the central wavelength and 3-dB spectral bandwidth were 1029 and 6.8 nm, respectively. The spectrum with steep edges display the typical characteristic of the all-normal-dispersion fiber lasers [36]. Figure 5B and inset show the corresponding oscilloscope trace. The interval between adjacent pulses is 26.8 ns, corresponding to a repetition rate and cavity length of 37.27 MHz and 5.48 m, respectively. The RF output spectrum (inset of Figure 5C) shows that the signal-to-noise ratio is 62 dB. The pulse width was deduced to be 10.15 ps from the autocorrelation trace (Figure 5D). The maximum output power is 37.9 mW, corresponding to a single-pulse energy of 1.017 nJ.

In order to verify the contribution of Ta_2NiS_5 SA in the mode-locking operation, we removed the SA and observed only the mode-locking phenomenon of NPE. The mode-locked pulse trains emerged when the pump power was increased to 120 mW. We measured the pulse duration as 6.6 ps, which is shorter than 10.15 ps. It implies that the insertion of SA has an impact on the loss and dispersion in the cavity, which will affect the output of mode locking.

4 Erbium-doped 1.5-μm fiber laser

The experimental setup is shown in Figure 6. The total length of the laser cavity is 4.53 m, corresponding to the dispersion of −0.076 ps^2, which contains a 56-cm Er-110-4/125 EDF. The oscillator also consists of a 980/1550

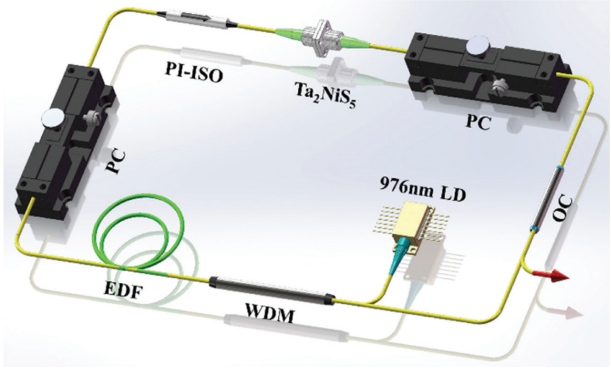

Figure 6: Diagram of the Erbium-doped fiber laser setup.

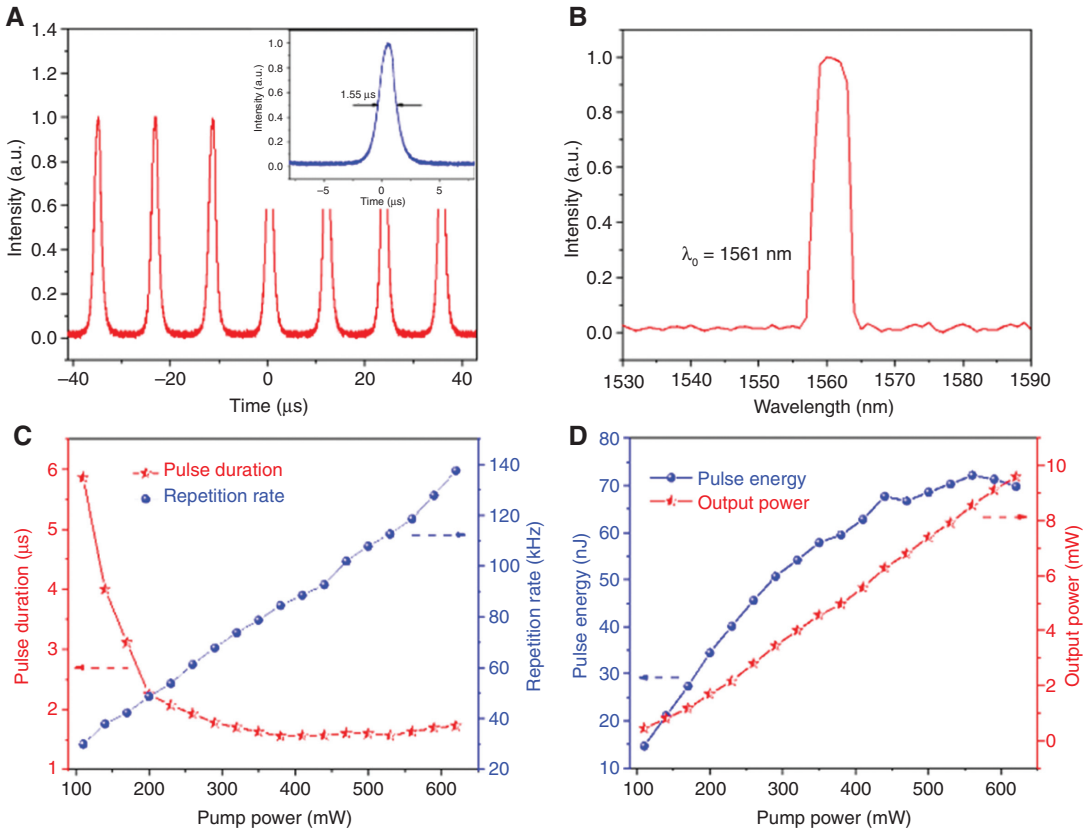

Figure 7: The results of Q-switched EDFL.
(A) Q-switched pulse width at the pump power of 390 mW. (B) Optical spectrum. (C) Pulse repetition rate and pulse duration vs. pump power. (D) Single-pulse energy and average output power vs. pump power.

wavelength-division multiplexer, a 10% OC, a PI-ISO, and a PC.

The output was connected to an optical spectrum analyser (HORIBA IHR550, Shanghai, China), a commercial autocorrelator (APE Pulse Check USB, Berlin, Germany), an RF spectrum analyzer (Agilent E4407B, CA, USA), and a real-time oscilloscope (Tektronix DPO3053, 500 MHz, 2.5 GS/S, Shanghai, China) together with a photodetector (Harmoniclaser UltraPD-1550, Yancheng, China), to allow measurements of the spectra and the pulse train.

4.1 Q-switched erbium-doped fiber laser (EDFL) with Ta_2NiS_5 SA

We could achieve self-starting Q-switching operation, generating a steady train of pulses (typical pulse characteristics are shown in Figure 7A with the minimum pulse duration of 1.55 μs, centered at 1561 nm (Figure 7B). By increasing the pump power, the repetition rate could be tuned from 30.02 to 137.6 kHz, whereas the corresponding pulse duration decreased from 5.8 to 1.72 μs (Figure 7C). Figure 7D shows the variation of the output power and single-pulse energy of the Q-switched EDFL vs. the pump power. As the pump power is raised from 110 to 620 mW, the output power increases from 0.44 to 9.6 mW, with an increase in pulse energy from 14.6 to 69.7 nJ and a maximum pulse energy of 72.11 nJ.

4.2 Mode-locked EDFL with Ta_2NiS_5 SA

In order to adjust the dispersion to realize mode-locking operation, we added a 65.44-m single-mode fiber in the cavity. Thus, there is a large negative dispersion of –1.45 ps^2 in the cavity, which is helpful for the formation of solitons.

Mode-locked pulses are generated when the pump power increases to about 150 mW. As presented in Figure 8A, the pulse repetition rate is about 2.92 MHz, which matches the cavity length well. Figure 8B depicts the RF spectrum with a resolution of 1 kHz; the signal-to-noise ratio is up to 67 dB. Figure 8C is the corresponding optical spectrum, whose 3-dB bandwidth is ~4.89 nm and the center wavelength is 1569 nm. The optical emission spectrum was recorded by an optical spectrum analyzer

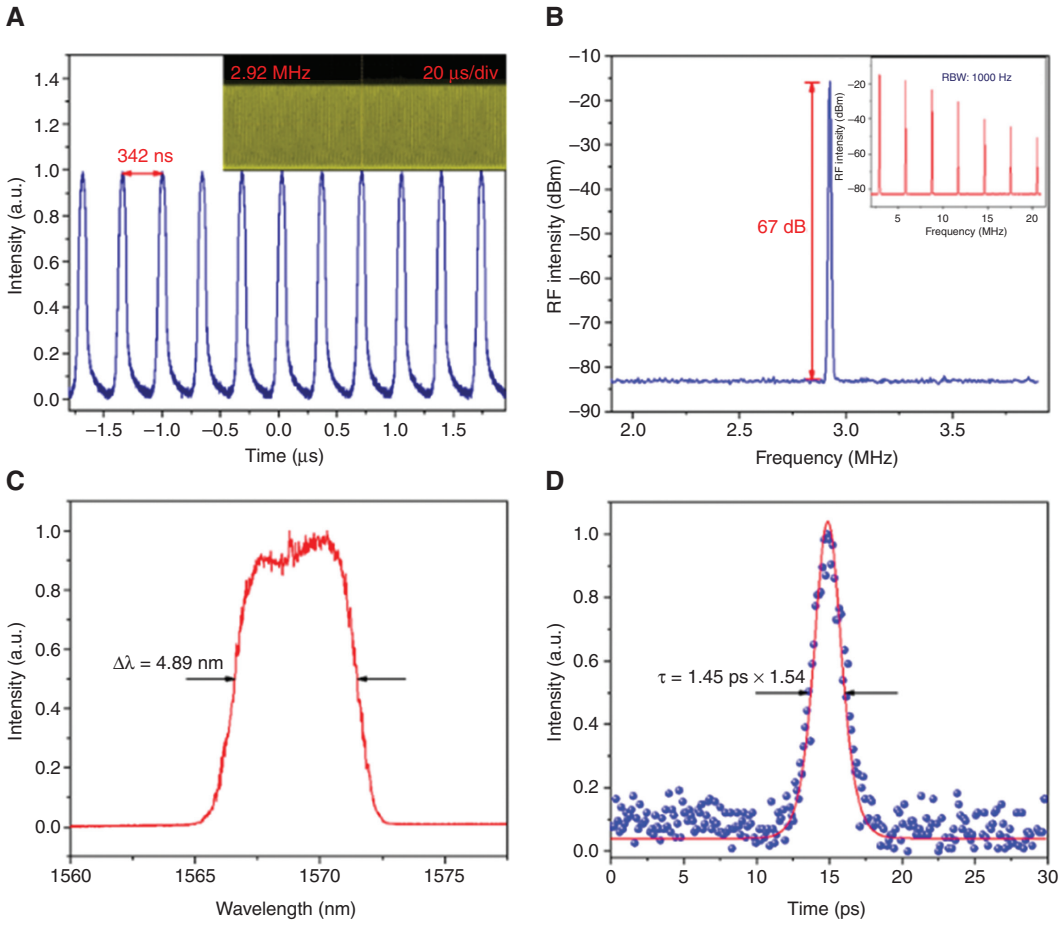

Figure 8: The results of mode-locked EDFL.
(A) Pulse trains of mode-locking operation at a pump power of 320 mW. Inset: Oscilloscope trace. (B) RF spectra. (C) Optical spectrum. (D) Autocorrelation trace for the output pulse.

Table 1: Comparison of the output performance of 1.5-μm mode-locked fiber laser based on various 2D materials.

SA	Repetition rate (MHz)	Pulse width (ps)	Output power (mW)	Single pulse energy (nJ)	Peak power	Wavelength (nm)	Reference
Sb_2Te_3	4.75	1.8	0.5	0.105	58 W	1558.6	[38]
rGO	16.79	1.17	3.16	0.18	161 W	1544.02	[39]
$PtSe_2$	23.3	1.02	12.3	0.53	519 W	1563	[40]
CuS_2	8.064	1.04	4.4	0.54	524 W	1530.4	[41]
TiS_2	5.34	1.04	26.9	5.05	4.85 kW	1569.5	[42]
Ta_2NiS_5	2.92	1.45	18.6	6.37	4.39 kW	1569	This work

(HORIBA IHR550) with a resolution of 0.05 nm. In addition, the fiber connected to the optical spectrum analyzer is a multimode fiber; so when the pulses are transmitted from the single-mode fiber to the multimode fiber, it can excite higher order modes and produce inter-mode interference, and thus the optical spectrum may not be as clean as would be expected. Figure 8D is the pulse autocorrelation trace, which can be well fitted by the $sech^2$ function, indicating that the real pulse width is 1.45 ps. The pulse broadening is attributed to the larger negative dispersion and the 1.5-m-long fiber pigtails used between the output coupler and the autocorrelator. Generally, higher modulation depth of the absorber will lead to shorter achievable output pulse duration [37].

In Table 1 we compare the Ta_2NiS_5-based SA with several nanomaterial-based SAs working around 1.5 μm. It can be seen that the maximum single-pulse energy of the mode-locked pulses obtained in this work is comparable

to that of other works described in Table 1. Thus, Ta_2NiS_5 is a promising material in high-energy pulsed laser generation.

5 Conclusions

In summary, stable passively Q-switched and mode-locked YDFL and EDFL were demonstrated using the ternary chalcogenide Ta_2NiS_5 as SA. The few-layer Ta_2NiS_5 was prepared by mechanical exfoliation. By inserting the Ta_2NiS_5-SA into different laser cavities, the Q-switched YDFL exhibited 1.07 μs minimum pulse duration and 117.2 nJ maximum pulse energy. The hybrid mode-locked YDFL achieved 10.15 μs pulse duration with an SNR of ~62 dB. And the Q-switched EDF laser was able to generate pulses with pulse energy of 72.11 nJ and minimum pulse duration of 1.55 μs. Stable mode-locked EDFL operation was successfully achieved with maximum pulse energy of 6.37 nJ and pulse width of 1.45 ps with a repetition rate of 2.92 MHz. These experimental results highlight the potential of Ta_2NiS_5 as a wideband SA for pulsed lasers and will greatly support 2D materials-based SA family.

Acknowledgment: This work was supported by the National Key R&D Program of China (No. 2018YFB1107200), the Open Research Fund of State Key Laboratory of Pulsed Laser Technology and the National Natural Science Foundation of China (No. 61675158 and 21673058, Funder Id: http://dx.doi.org/10.13039/501100001809), the Singapore National Research Foundation under NRF award number NRF-RF2013-08, Tier 2 MOE2015-T2-2-007, MOE2015-T2-2-043, MOE2017-T2-2-136, and the A*Star QTE program.

References

[1] Skorczakowski M, Swiderski J, Pichola W, et al. Mid-infrared Q-switched Er:YAG laser for medical applications. Laser Phys Lett 2010;7:498.
[2] Luo Z, Huang Y, Zhong M, et al. 1-, 1.5-, and 2-μm fiber lasers Q-switched by a broadband few-layer MoS_2 saturable absorber. J Lightwave Technol 2014;32:4077.
[3] Piao Z, Zeng L, Chen Z. Q-switched erbium-doped fiber laser at 1600 nm for photoacoustic imaging application. Appl Phys Lett 2016;108:143701.
[4] Song Y, Liang Z, Jiang X, et al. Few-layer antimonene decorated microfiber: ultra-short pulse generation and all-optical thresholding with enhanced long term stability. 2D Mater 2017;4:045010.
[5] He J, Dong H, Deng R. Low-cost bidirectional hybrid fiber-visible laser light communication system based on carrierless amplitude phase modulation. Opt Eng 2016;55:086109.
[6] Song YF, Li L, Tang DY, Shen DY. Quasi-periodicity of vector solitons in a graphene mode-locked fiber laser. Laser Phys Lett 2013;10:125103.
[7] Xu Y, Wang Z, Guo Z, et al. Solvothermal synthesis and ultrafast photonics of black phosphorus quantum dots. Adv Opt Mater 2016;4:1223–9.
[8] Liu W, Li M, Yin J. Tungsten diselenide for all-fiber lasers with chemical vapor deposition method. Nanoscale 2018;10:7971.
[9] Matsas VJ, Newson TP, Richardson DJ. Selfstarting passively mode-locked fibre ring soliton laser exploiting nonlinear polarisation rotation. Electron Lett 1992;28:1391.
[10] Song Y, Shi X, Wu C, Tang D, Zhang H. Recent progress of study on optical solitons in fiber lasers. Appl Phys Rev 2019;6:021313.
[11] Keller U. Recent developments in compact ultrafast lasers. Nature 2003;424:831.
[12] Zhang H, Bao Q, Tang D, Zhao L, Loh K. Large energy soliton erbium-doped fiber laser with a graphene-polymer composite mode locker. Appl Phys Lett 2009;95:141103.
[13] Guo Z, Zhang H, Lu S, et al. From black phosphorus to phosphorene: basic solvent exfoliation, evolution of Raman scattering, and applications to ultrafast photonics. Adv Funct Mater 2015;25:6996–7002.
[14] Luo Z-C, Liu M, Guo Z-N, et al. Microfiber-based few-layer black phosphorus saturable absorber for ultra-fast fiber laser. Opt Express 2015;23:20030–9.
[15] Chen Y, Jiang G, Chen S, et al. Mechanically exfoliated black phosphorus as a new saturable absorber for both Q-switching and mode-locking laser operation. Opt Express 2015;23:12823.
[16] Qin Z, Xie G, Zhang H, et al. Black phosphorus as saturable absorber for the Q-switched Er:ZBLAN fiber laser at 2.8 μm. Opt Express 2015;23:24713–8.
[17] Ma J, Lu S, Guo Z, et al. Few-layer black phosphorus based saturable absorber mirror for pulsed solid-state lasers. Opt Express 2015;23:22643–8.
[18] Song Y, Chen S, Zhang Q, et al. Vector soliton fiber laser passively mode locked by few layer black phosphorus-based optical saturable absorber. Opt Express 2016;24:25933–42.
[19] Zhang Y, Zhu J, Li P. All-fiber Yb-doped fiber laser passively mode-locking by monolayer MoS_2 saturable absorber. Opt Commun 2018;413:236.
[20] Chen B, Zhang X, Guo C. Tungsten diselenide Q-switched erbium-doped fiber laser. Opt Eng 2016;55:081306.
[21] Li J, Zhao Y, Chen Q. Passively mode-locked ytterbium-doped fiber laser based on SnS_2 as saturable absorber. IEEE Photon J 2017;9:1.
[22] Wang Y, Liu S, Yuan J. Ultra-broadband nonlinear saturable absorption for two-dimensional $Bi_2Te_xSe_{3-x}$ nanosheets. Sci Rep 2016;6:33070.
[23] Tani S, Blanchard F, Tanaka K. Ultrafast carrier dynamics in graphene under a high electric field. Phys Rev Lett 2012;109:166603.
[24] Gao T, Zhang Q, Li L, et al. 2D ternary chalcogenides. Adv Opt Mater 2018;6:1800058.
[25] Mu K, Chen H, Li Y. Electronic structures of layered Ta_2NiS_5 single crystals revealed by high-resolution angle-resolved photoemission spectroscopy. J Mater Chem C 2018;6:3976.
[26] Sunshine SA, Ibers JA. Structure and physical properties of the new layered ternary chalcogenides tantalum nickel sulfide

(Ta_2NiS_5) and tantalum nickel selenide (Ta_2NiSe_5). Inorg Chem 1985;24:3611.
[27] Li L, Gong P, Wang W. Strong in-plane anisotropies of optical and electrical response in layered dimetal chalcogenide. ACS Nano 2017;11:10264.
[28] Ahmad H, Reduan SA, Aidit SN. Generation of passively Q-switched fiber laser at 1 μm by using MoSSe as a saturable absorber. Chin Opt Lett 2017;15:15.
[29] Nicolosi V, Chhowalla M, Kanatzidis MG. Liquid exfoliation of layered materials. Science 2013;340:1226419.
[30] Zhang C, Liu M, Man BY. Facile fabrication of graphene-topological insulator Bi_2Se_3 hybrid dirac materials via chemical vapor deposition in Se-rich conditions. Cryst Eng Commun 2014;16:8941.
[31] Liu H, Zheng XW, Liu M. Femtosecond pulse generation from a topological insulator mode-locked fiber laser. Opt Express 2014;22:6868.
[32] Han X, Zhang H, Zhang C. Large-energy mode-locked ytterbium-doped linear-cavity fiber laser based on chemical vapor deposition-Bi_2Se_3 as a saturable absorber. Appl Opt 2019;58:2695.
[33] Yan B, Zhang B, He J. Ternary chalcogenide Ta_2NiS_5 as a saturable absorber for a 1.9 μm passively Q-switched bulk laser. Opt Lett 2019;44:451.
[34] Tan C, Yu P, Hu Y, et al. High-yield exfoliation of ultrathin two-dimensional ternary chalcogenide nanosheets for highly sensitive and selective fluorescence DNA sensors. J Am Chem Soc 2015;137:10430–6.
[35] Ma M, Wen W, Zhang Y. Few-layer $ReS_{2(1-x)}Se_{2x}$ nanoflakes for noise-like pulse generation in a mode-locked ytterbium-doped fiber laser. J Mater Chem C 2019;7:6900.
[36] Chong A, Renninger WH, Wise FW. Properties of normal-dispersion femtosecond fiber lasers. J Opt Soc Am B 2008;25:140.
[37] Jeon J, Lee J, Lee JH. Numerical study on the minimum modulation depth of a saturable absorber for stable fiber laser mode locking. J Opt Soc Am B 2015;32:31–7.
[38] Sotor J, Sobon G, Macherzynski W. Mode-locking in Er-doped fiber laser based on mechanically exfoliated Sb_2Te_3 saturable absorber. Opt Mater Express 2014;4:1.
[39] Ahmad H, Soltani S, Thambiratnam K. Mode-locking in Er-doped fiber laser with reduced graphene oxide on a sidepolished fiber as saturable absorber. Opt Fiber Technol 2019;50:177.
[40] Zhang K, Feng M, Ren Y. Q-switched and mode-locked Er-doped fiber laser using $PtSe_2$ as a saturable absorber. Photon Res 2018;6:68.
[41] Hui Z, Xu W, Li X. Cu_2S nanosheets for ultrashort pulse generation in near-Infrared regions. Nanoscale 2019;11:6045.
[42] Ge Y, Zhu Z, Xu Y. Ultrafast photonics: broadband nonlinear photoresponse of 2D TiS_2 for ultrashort pulse generation and all-optical thresholding devices. Adv Opt Mater 2017;6:1701166.